ICAS 2020 SHANGHAI
International Council of the Aeronautical Sciences
32nd Congress of the International Council of the Aeronautical Sciences
September 6-10, 2021
Pudong Shangri-La, Shanghai, China

HIGH-LIFT NOISE REDUCTION USING PLASMA ACTUATORS

Gabriel Pereira Gouveia da Silva[1], João Paulo Eguea[1], José Antonio Garcia Croce[2] & Fernando Martini Catalano[1]

[1]Department of Aeronautical Engineering, University of São Paulo, Brazil
[2]Federal Institute of Education, Science and Technology of São Paulo, Brazil

Abstract

During the approach, high-lift devices are among the major sources of aircraft noise. Most of the current solutions are based on passive flow control technologies, which are reaching a limit of their noise reduction performance. Thus, devices based on active flow control may allow for additional improvements. One way of doing active flow control is through the use of dielectric barrier discharge plasma actuators. These devices produce a wall jet by ionizing and accelerating the air nearby through an intense electric field. In this research, dielectric barrier discharge plasma actuators were installed at a flap rounded tip (to reduce the strength of the side-edge vortices), at the cove and the cusp of a leading-edge slat (to change the shear layer behavior). A parametric study was carried out varying plasma actuator geometry, plasma actuator position of installation, voltage, frequency, duty cycle, and modulation frequency. Far-field acoustic array and surface pressure measurements in a wind tunnel were conducted and the results demonstrated the potential of plasma actuators for high-lift noise reduction. A decrease of up to 0.75 dB in the overall flap noise and up to 3.3 dB in the overall slat noise (with 12 dB of reduction in the dominant tonal peak) were achieved by using the plasma actuators. However, many configurations were not able to reduce or even has increased the overall noise, evidencing the need of proper optimization of the plasma actuator geometry, materials, and operational parameters to improve the control authority of these devices.

Keywords: airframe noise, active flow control, dielectric barrier discharge, electrohydrodynamics, aeroacoustics

1. Introduction

With the expansion of urbanized areas and the growth of aircraft operations, aeronautical noise has negatively impacted an increasing number of people, which has led regulatory authorities to adopt increasingly restrictive levels of acceptable aircraft noise [1]. Until the 1970s aircraft noise generation was dominated by the propulsion system, but this noise source has been constantly reduced with the increase in the bypass ratio of the turbofan engines [1, 2, 3]. So, in phases of flight when the engine operating power is low (as during the approach), airframe noise has become dominant [1, 2, 3]. Airframe noise is generated by the interaction of the external turbulent flow with exposed geometrical discontinuities of the aircraft non-propulsive surfaces [2, 4, 3]. The high-lift devices are among the most relevant airframe noise sources [1, 2, 5]. Broadband noise with frequencies up to 2.5 kHz is generated at the leading edge slat and broadband noise with frequencies from 4 to 16 kHz is produced at the flap [6, 7, 8].

1.1 Slat noise

Slat noise is generated by a combination of overlapping phenomena and is a complex aeroacoustic problem not yet fully understood [9, 10]. It is predominantly a broadband noise source at flight conditions, although wind tunnel models show the occurrence of tonal peaks that are not observable in flight [11, 12, 13]. The flow inside the cove of the slat depends strongly on its geometry, deflection angle, gap, overlap, flow speed, and angle of attack of the wing [14, 15]. When the slat is extended,

there is a region of flow separation in its cove in which instabilities and vorticities are generated and interact with the nearby surfaces, generating noise [14, 16, 13]. This vorticity is produced and fed by the flow that passes through the slot and, between this cove vortex the undisturbed flow, a free and unstable shear layer appears [14, 16, 13]. This shear layer originates at the slat cusp and impinges the surface of the slat cove in the reattachment point [14, 16, 13]. This shear layer is a natural amplifier of low and medium frequency disturbances due to a feedback loop described in more detail in the literature [16, 17, 18, 19, 3], and it probably gives rise to the instabilities that cause slat noise [9, 20, 21]. The vortices shed from the cusp are convected through the shear layer and suffer strong and rapid distortions along its path, especially near the reattachment point [16, 17, 18, 19]. The strong pressure fluctuations caused by the interaction of these distorted vortices with the trailing edge of the slat are an important source of slat noise [14, 18, 22]. In addition, low-frequency noise components can be generated due to the non-stationarity of the vortex contained inside the slat cove [16, 13]. Other possible noise sources, mainly when it comes to wind tunnel models, are associated with the vortex shedding at the slat trailing edge (high-frequency tonal peaks) and with the coherent laminar separation with vortex shedding at the slat cusp (low-frequency tonal peaks) [9, 16, 13, 19, 23, 24, 11, 25].

1.2 Flap noise

The flap noise is generated by complex three-dimensional vortices: due to static pressure difference between suction and pressure surfaces of the flap side-edge, a primary vortex develops at the lower edge from the pressure to the suction side of the flap, near its leading edge; for the same reason, a secondary vortex develops from the flap upper edge to its suction side [26, 27, 13, 5]. The lower vortices are continuously fed by the shear layer instabilities and are drawn by the flow to the upper surface, where both these vortices are merged and then separate from the pressure side at some position around 70% of the flap chord [26, 27, 13, 5]. So, the flap noise is a combination of classical leading edge noise mechanisms, pressure fluctuations caused by vortex breakdown, interaction between vortices and surfaces or edges, and accelerated free turbulence in the vortex flow [27, 13, 28, 5]. Therefore, the flap is mainly a broadband noise source where unsteady vorticity fluctuations from pressure side shear layer interacting with the upper tip edge produce mid-to-high frequencies, and vortex interaction with suction side surface after vortex merging produces low-to-mid frequencies [27, 28]. The total noise radiated from flap is higher at higher flap deflection angles [6]. Thus, the intensity of sound radiation depends upon the strength of the vorticity at the flap side-edges and the distance of the vortex from the edges, therefore a reduction in the tip vortex intensity could reduce the noise radiated from the flap tip [29].

1.3 Solutions for high-lift aerodynamic noise

Passive flow control is the basic principle behind most of the devices currently used to reduce high-lift aerodynamic noise [20, 6, 16, 27, 31, 15, 13, 4, 32, 8, 30, 33, 5]. These devices, however, can degrade aerodynamic performance, be heavy, mechanically complex, and difficult to manufacture and maintain [13]. Besides, Young et al. [34] noted that the Advisory Council for Aeronautics Research in Europe (ACARE) noise reduction target would not be reached, considering the trend of asymptotic improvement achieved by the passive flow control solutions to airframe noise currently adopted by the industry. In this way, Young et al. [34] recommend that technologies based on active flow control should be sought. The researches on airframe noise reduction through active flow control devices, however, have a low technology readiness level (TRL), which can be improved by developing more research on these topics [34, 3]. Active flow control is achieved by manipulating the airflow through an energy addition to it (for example, using dielectric barrier discharge plasma actuators, also known as DBD-PAs) [3].

1.4 Dielectric barrier discharge plasma actuators

DBD-PAs are electric devices that convert directly electric energy into flow kinetic energy, producing a jet in the proximity of their surface without using pneumatic, hydraulic, or moving parts [35, 36, 3]. DBD-PAs have low weight, low thickness, fast response, and low power consumption, being appropriate for aerodynamic control [35, 36]. They are usually made of two flat electrodes mounted

on opposite sides of a dielectric layer (Figure 1), which are subjected to a high AC voltage (usually from a few kV to 30 kV, with frequencies ranging from 100 Hz to a few tens of kHz) [35, 36, 3].
The intense electric field generated by the high AC voltage applied to the DBD-PA electrodes ionizes the air near the encapsulated electrode, producing an atmospheric cold plasma that is accelerated by the same electric field [37, 3]. A suction region appears over the exposed electrode and draws the surrounding air toward the wall, from where it is then ejected tangentially to the surface, from the exposed electrode edge, and over the region of the encapsulated electrode, thereby inducing a pseudo wall jet [38, 39, 40, 3]. Since only momentum is injected into the flow (and not mass), the jet induced by the DBD-PA is different from the classic wall jet [36, 40]. Due to the large differences in the spatial and temporal discharge structures between the positive and negative halves of the voltage applied to the electrodes, the jet induced by the DBD-PA has a preferential direction that depends on the orientation of the asymmetrically arranged electrodes [41, 3]. According to several studies, the negative half of the discharge cycle induces a higher horizontal velocity, being responsible for about 97% of the momentum coupling, which causes the DBD-PA jet to be unidirectional despite the AC voltage applied [42, 43, 37, 35, 41, 36, 3].
The electrical and mechanical characteristics of the plasma-induced jet are strongly dependent on several constructive and operational factors [3]. According to a literature review carried out by Silva et al.[3], the most relevant constructive parameters that influence the DBD-PAs performance are the dimensions and shape of the electrodes, the gap between the electrodes, the dielectric thickness, and the dielectric material, whereas the main operational parameters that affect the performance of the DBD-Pas are the applied voltage, the AC frequency, the voltage waveform, the duty cycle, and the unsteady modulation frequency. The relation between these parameters and the actuator performance is highly interdependent and non-linear, which complicates the design, optimization, and mathematical modeling of the DBD-PAs. Nonetheless, Silva et al. [3] list several works published considering the individual influence of each parameter on the DBD-PA performance, which can be a guide for building and operating these devices.
As highlighted by Silva et al. [3] in its literature review, most of the existing applications of DBD-PAs are related to aerodynamic performance improvements (for example, lift-to-drag ratio rise, drag reduction, and stall delay) caused by transition control and boundary layer separation delay through vortex generation and momentum addition. One of these applications that could be related to high-lift devices was published by He et al. [44], who used DBD-PAs for delaying the stall. These researchers used DBD-PAs installed on the leading edge of a wing to keep the flow attached at high angles of attack [44]. This way, the DBD-PAs could replace the complex and heavy mechanisms of flaps and slats[44], which would be especially advantageous for aircraft design due to the possibility of weight and high-lift noise reduction [44, 3]. However, Silva et al. [3] have listed some problems related to this concept, such as the high risk of a stall at low altitudes in case of DBD-PA failure, and the lack of control authority under real flight scale conditions. Thus, Silva et al. [3] mention that the conventional high-lift devices are more reliable, being more feasible for new aircraft designs [3]. Thus, finding a solution that combines traditional flaps and slats with plasma actuators to attenuate their noise is more interesting from a commercial point of view since the risk of compromising the flight safety is reduced [3]. Young et al. [34] mention a concept proposed by research groups from the University of Notre Dame and Airbus Noise Technology Center in which a combination of flap rounded tip and plasma actuators could guide the tip vortices away from the flap side-edge, thereby reducing noise. However, to date, it was not found in the literature the development of this concept. Thus, a concept similar to that mentioned by Young et al. [34] was developed and tested in a wind tunnel, the results being presented hereby. The difference here is that the DBD-PAs were used not to blow the vortex away from the flap, but to generate a counter-vortex in combination with the flap rounded tip. The idea of using DBD-PAs to produce a counter-vortex at the flap tip was inspired by the work developed by Hasebe et al. [45], who applied a similar configuration to reduce induced drag in a wing, and the purpose of the rounded tip was to facilitate the production of this counter-vortex by inducing a Coandă-like effect.
The purpose of this research was to test if DBD-PAs can be used to reduce flap side-edge noise by reducing the side-edge vortices strength. This work is part of the same research project [3] in which

the ability of DBD-PAs in reducing leading-edge slat noise was demonstrated.

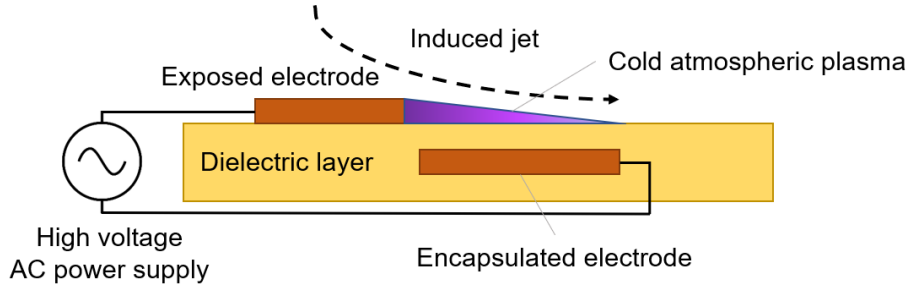

Figure 1 – Schematic cross section of a conventional DBD-PA (out of scale).

2. Experimental setup and procedures

The experimental setup and procedures used to assess the ability of the DBD-PA as a solution to slat and flap noises are briefly presented in this section and are thoroughly reported in Silva et al. [3] and Silva [46].

2.1 Wind tunnel and microphone array

The acoustic array measurements were carried out at the LAE-1 wind tunnel, at the Department of Aeronautical Engineering of the University of São Paulo (Brazil). It is a closed-circuit low-speed wind tunnel, with a closed test section of 1.3 m height, 1.67 m width and 3.0 m length [3]. It operates at an airspeed up to 50 m/s with a turbulence level up to 0.21% [47, 48, 49, 3]. Acoustic treatments made by Santana et al. [49] reduced the LAE-1 wind tunnel background noise by 5 dB and practically removed the fan tonal peaks [3]. Considering that the LAE-1 wind tunnel has a hard-wall closed test section, a phased array technique was used to improve the signal-to-noise ratio of the acoustic [3]. The microphone array used has 61 G.R.A.S. 46BD microphone sets, flush-mounted without grid at the test section side-wall in a modified spiral distribution (Figure 2) for high-frequency range with minimum beamwidth and side-lobe contamination [50, 3].

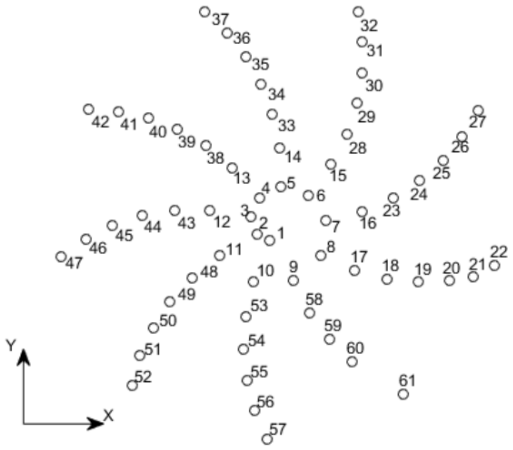

Figure 2 – Microphone array geometry [46]

These microphones have a frequency range of 4 Hz to 70 kHz, a dynamic range of 166 dB, and a calibrated sensitivity of 1.5 to 2.6 mV/Pa (measured for each microphone using a Rion NC-74 calibrator) [3]. This set of geometry and configurations ensures an array beamwidth (spatial resolution) smaller than 100 mm for frequencies above 400 Hz and a frequency resolution of 25 Hz [51, 3]. The synchronization and acquisition of the microphone signals were done through a National Instruments NI PXIe system, whose technical specifications can be found in details at Silva et al. [3] or Silva [46]. Data acquisition, processing, and storage were executed through a MATLAB program developed by Pagani Júnior [51]. Atmospheric pressure, temperature, and relative humidity were measured with

analog instruments at the beginning of each test and were manually input into the code. The dynamic pressure measurements from a DP-Calc 8705 Micromanometer and the microphones measurements synchronized by the NI PXIe system are automatically registered by the program. The raw data were then processed with a frequency domain beamforming code (also implemented by Pagani Júnior [51]) in the same way as in [3]. The code performs a Fast Fourier transform of microphone measurements through Welch's methodology with 50% of block overlap and Hanning windowing, correcting the power by a factor of 8/3 [51, 52, 3]. The process is repeated for all the microphones to create a Cross Spectral Matrix (CSM), from which conventional beamforming calculations are made through a spatial filter within a selected potential source location, using steering vector normalization [51, 52, 3].

2.2 High-voltage AC power supply and plasma actuators

The high-frequency high-voltage AC power supply (HFHVPS) used was the same as in [3]. It is an in-house equipment that can provide up to 23.0 kV AC at 6.0 kHz. It consists of a high-frequency wave generator coupled to a high-voltage transformer, both supplied by a commercial DC power supply [3]. For complete information about the HFHVPS, including its circuit diagram and Arduino code, see reference [46].

The plasma actuators were made of hand-cut and hand-laid self-adhesive tapes of copper foil (0.045 mm thick) and polyimide film (0.054 mm thick per layer). One layer of polyimide film was used as a substrate and three layers of polyimide film were used as the dielectric between the exposed and the encapsulated electrodes. The geometries chosen for the DBD-PA tested in the slat were detailed at reference [3] and are not reproduced here due to copyright issues. The geometry chosen for the flap was the traditional straight electrode configuration, with dimensions shown in Figure 3. The chordwise extension of the electrodes was of 20 mm. This DBD-PA was able to induce a 1 m/s jet in quiescent air [46, 3].

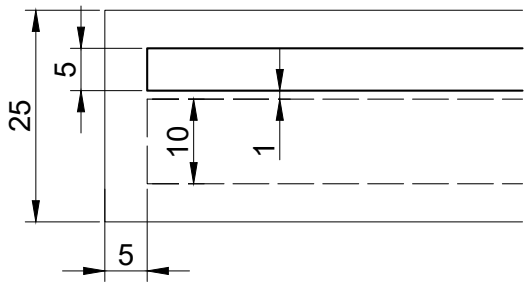

Figure 3 – Straight electrode DBD-PA dimensions [mm].

2.3 Wind tunnel models and experimental procedures

The slat scaled model tested and the positions where the DBD-PAs were installed on it were detailed at reference [3] and are not reproduced here due to copyright issues. The flap scaled model used is representative of a conventional aircraft flap. It was designed and built by [33]. It was built by assembling laser-cut MDF ribs, steel spars, and an aluminum alloy skin. At 10 mm from the original flap tip (Figure 5), 57 pressure taps distributed chordwise along the flap surface (Figure 4) are connected to plastic tubes that pass inside the flap. The flap chord has 700 mm in order to have higher Strouhal and Reynolds numbers, since scaling is a problem in aeroacoustic wind tunnel testing, and the span has 700 mm.

In order to induce a Coandă-like effect at the flap tip with the ionic blowing from the DBD-PAs, a rounded tip for the flap model was designed and built. This tip was made of PLA through fused filament fabrication (FFF) and have received a finishing with primer, sandpaper, and painting. It has a hollow section for both material saving and housing the wires. Two circular holes and a central joint are used to position and fix the rounded tip at the flap model.

Four configurations were tested, varying the installation position of the DBD-PAs on the flap rounded tip. In each position, two DBD-PAs were connected in parallel, one in the suction side, blowing spanwise away from the flap tip and the other in the pressure side, blowing spanwise towards the

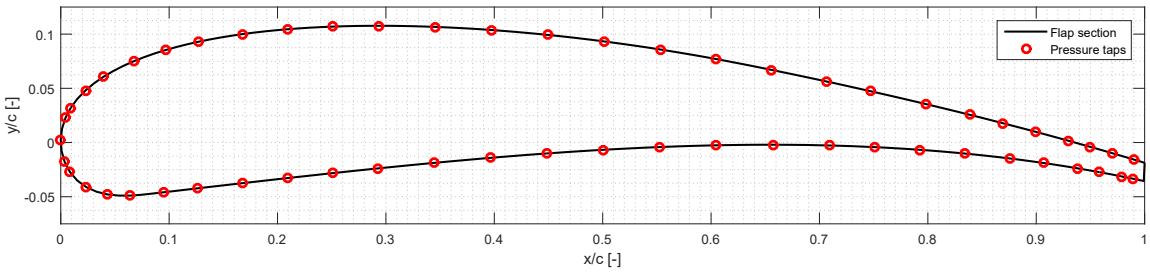

Figure 4 – Flap section and pressure taps (based on data from [33]).

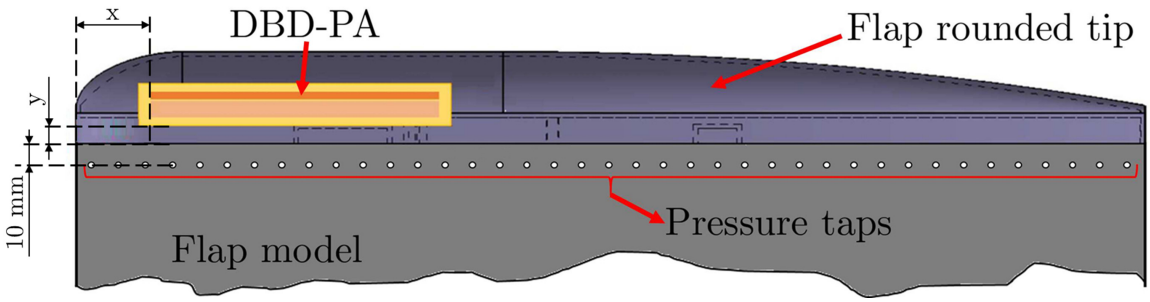

Figure 5 – Pressure taps and DBD-PA position at the flap tip.

flap root (Figure 7). The position of the electrodes for each one of four configurations are presented in Table 1, with x/c and y/c defined in Figure 5.

Position	x/c [%]	y/c [%]
1	7.1	0.0
2	38.6	0.0
3	7.1	5.7
4	38.6	3.6

Table 1 – DBD-PAs position on the flap rounded tip (each position has two DBD-PA, one at the suction side, one at the pressure side.

Finally, the flap was fixed to the turning table at the middle of the wind tunnel test section, facing the microphone array (Figure 6). The DBD-PA wires and the pressure tubes pass through the model out of the tunnel. The pressure measurements at the model were made through a Scanivalve ZOC-33/64PxX2 electronic pressure scanning module. It has a 2.5 kPa full-scale range, 10 in $H_2O \pm 0.15\%$ FS accuracy and a 40 kHz scan rate. The tubes coming from the pressure taps were connected to the ScaniValve module, which communicated with a computer for the data acquisition through FTP protocol. The dynamic pressure of the wind tunnel flow was measured by a Pitot tube and a static pressure tap both connected to a micromanometer DP-Calc 8705 [3]. It has a full-scale range of -1.245 kPa to 3.735 kPa, with an accuracy of 1% of the reading $\pm$ 1 Pa [3]. The micromanometer acquisition was made by the National Instruments PXIe system described in section 2.1
All the tests were carried out with the angle of attack set to $26°$. This choice was made to achieve the same aerodynamic loading the flap would have if the complete multi-element wing were present at zero angle of attack [33, 30]. For further details on this consideration, the reader can consult references [33] and [30]. The acoustic array measurements were made with a 102.4 kHz sample rate during 20 s of measurement time (which ensures an error of $\pm$ 0.02 dB in the overall sound pressure level [52, 3]). Each one of the four configurations was tested for all the combinations listed in Table 2.For details on the complete experimental setup and test matrix of the experiments with DBD-PAs installed at the slat, the reader can refer to [3].

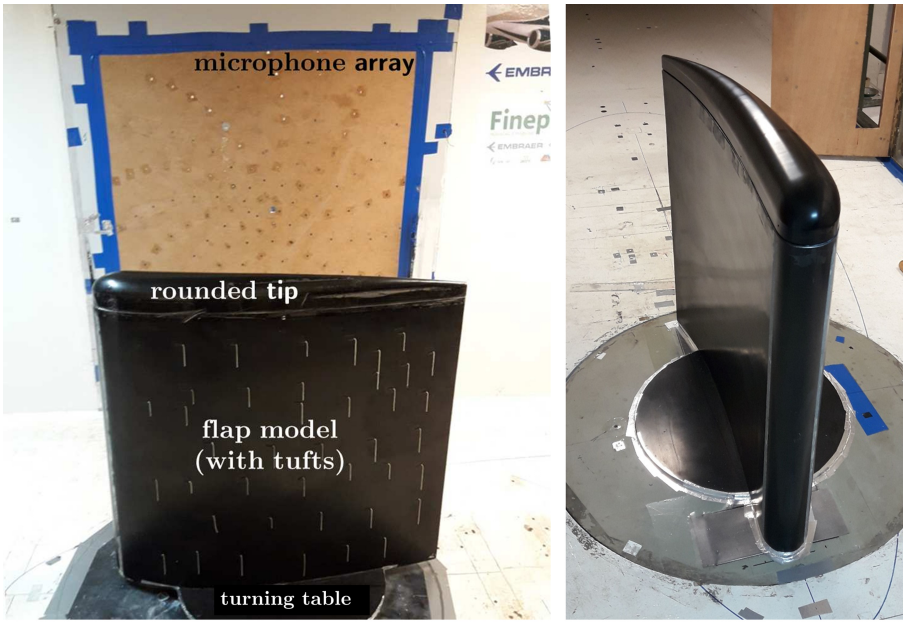

Figure 6 – Flap model installed at the test section of the LAE-1 wind tunnel.

Figure 7 – DBD-PAs connected in parallel, the arrows illustrate the direction of the jets produced.

3. Results

The analysis of the results is conducted in the same way as in a previous work of published by the authors [3]. For each configuration tested (Table 2) the overall sound pressure level difference (ΔOASPL) between the measurements with the DBD-PA activated and deactivated was plotted. When the DBD-PAs reduced the OASPL, the integrated power spectral density (PSD) and the difference in PSD between the activated and deactivated conditions are shown for the best configurations in each position. When the DBD-PAs only worsened the overall noise, the spectra of the worst configurations are presented. The surface pressure distributions at the flap tip, which indicate the vortices position and strength, are also presented.

The ΔOASPL between each configuration and the baseline (DBD-PAs installed but deactivated) was calculated from the acoustic beamforming outputs of the processing described by Silva et al. [3]. As in our previous work [3], to avoid the contamination of the high frequency DBD-PA actuation self-noise in the analysis, the sound spectra presented hereby were truncated at the plasma actuation frequency and the ΔOASPL obtained after the truncation is noted as ΔOASPL*. This procedure is the same used by [3] and is valid due to the actual flight scale frequency ranges of the flap noise, which are much smaller than those produced by a scaled model in wind tunnel (for the same Strouhal number), whereas the high frequencies of the DBD-PA actuation noise would be the same either for

	$Re = 1.12 \times 10^6$, $M = 0.08$	$Re = 5.76 \times 10^5$, $M = 0.04$
α	26°	26°
Position	1 and 2	3 and 4
V_{in}	30 V (DC)	30 V (DC)
f	3.0, 4.0, 5.0, 6.0, 7.0 and 7.9 kHz	3.0, 4.0, 5.0, 6.0, 7.0 and 7.9 kHz
F	10 Hz	10 Hz
D.C.	50%, 75% and 100%	50%, 75% and 100%
Measurements	Acoustic array and chordwise surface pressure	Acoustic array and chordwise surface pressure

Table 2 – Flap side-edge test matrix.

real flight conditions or for wind tunnel scaled conditions [3]. These ΔOASPL* values are presented at Figure 8. Then, sound spectra (integrated PSD), PSD difference and pressure distribution at the flap tip are shown for the best and the worst cases, to provide an understanding of how the DBD actuation affected the flap side-edge noise generation mechanism.

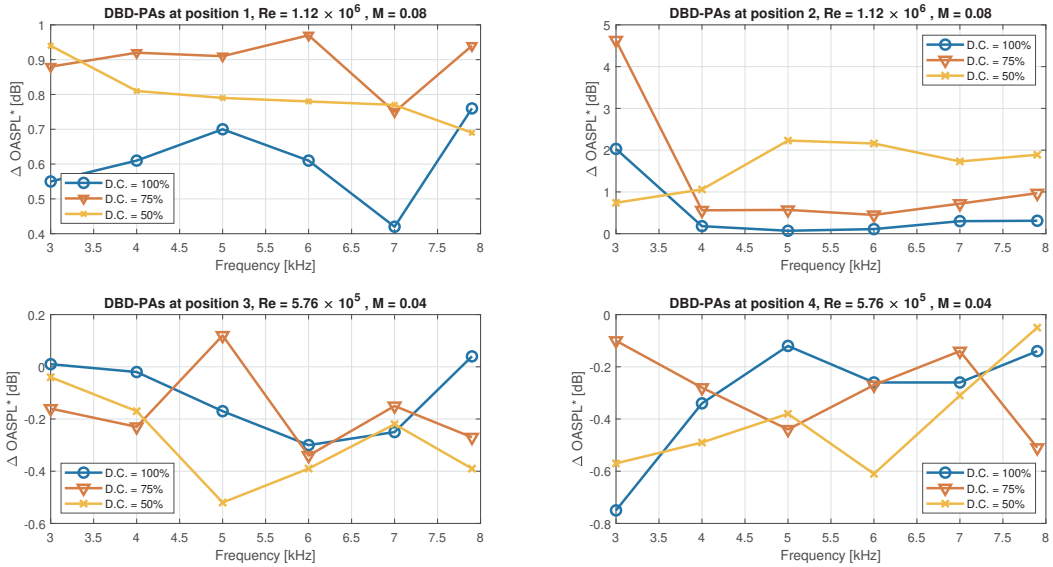

Figure 8 – Overall sound pressure level difference between the conditions with DBD-PAs activated and deactivated.

From data depicted in Figure 8, it is evident that the positions 1 and 2, which were tested at higher Reynolds number, were not effective in reducing aerodynamic noise. Instead, they were all prejudicial, since the overall sound pressure level was increased by the DBD-PAs activation for all the combinations of configurations tested.

For position 1, the worst configuration tested was with a frequency of $6.0\ kHz$ and modulated at $F = 10\ Hz$, with a duty cycle of 75%. From Figure 9, it can be seen that the plasma actuation has increased the broadband noise for most frequencies. In the Figure 11, a small rise in a suction point was observed at the region where de DBD-PAs were installed, whereas the pressure side was affected downstream the plasma actuators, where the pressure coefficient was approached to zero when DBD-PAs were activated in relation to the baseline condition.

For position 2, the worst configuration tested was with a frequency of $3.0\ kHz$ and modulated at $F = 10\ Hz$, with a duty cycle of 75%. From Figure 10, it can be seen that the plasma actuation in these conditions has introduced some tonal noise with harmonics of the frequencies of $520\ Hz$ and $1080\ Hz$. Figure 11 depicts the effect of plasma actuation on the pressure distribution affected by the vortices system. A small rise in the peak of suction was observed. At the region where the DBD-PAs were installed, the vortex was reduced (there is a reduction of the suction from x/c 0.4 to 0.7). The pressure side upstream the DBD-PAs was also affected, raising its pressure.

In the case of positions 3 and 4, tested at lower Reynolds, Figure 8 shows a more effective result

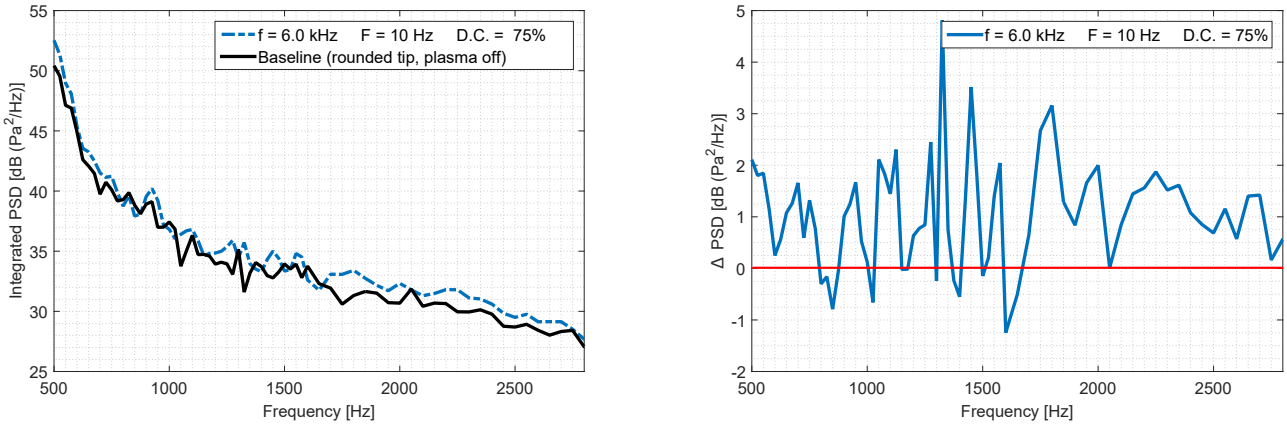

Figure 9 – Sound spectra: DBD-PAs installed at position 1, $V_{in} = 30\ V$ ($V_{pp} = 22.8\ kV$), $\alpha = 26°$, $Re = 1.12 \times 10^6$, $M = 0.08$.

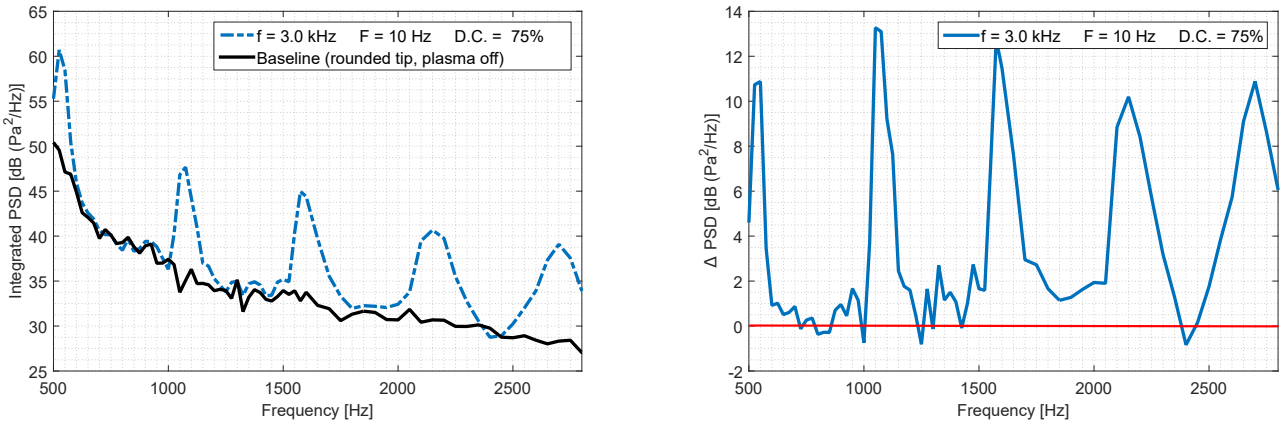

Figure 10 – Sound spectra: DBD-PAs installed at position 2, $V_{in} = 30\ V$ ($V_{pp} = 9.4\ kV$), $\alpha = 26°$, $Re = 1.12 \times 10^6$, $M = 0.08$.

of plasma actuation. This difference may be related to the problem of the DBD-PA control authority loss when Reynolds number is increased, as reported by other researchers. Although the results for positions 3 and 4 are of overall sound pressure level reduction, the benefit is still marginal. For position 3, the best configuration tested was with a frequency of $5.0\ kHz$ and modulated at $F = 10\ Hz$, with a duty cycle of 50%. From Figure 12, it can be seen that some marginal improvement was achieved. For some frequencies, the PSD difference was up to $-5\ dB$, but for other frequencies, a rise of up to $3\ dB$ was produced. Figure 14 depicts the effect of plasma actuation on the pressure distribution affected by the vortices system. Practically no effect on the peak of suction was observed for the position 3. At the region where the DBD-PAs were installed, the pressure coefficient was augmented from x/c 0.2 to 0.4 at the pressure side. The vortex downstream the DBD-PAs was shifted towards the leading edge, as can be seen by the suction region from the left graph at the Figure 14. Finally, considering the position 4, the best configuration tested was with a frequency of $3.0\ kHz$ and steady actuation (duty cycle of 100%). From Figure 13, it can be seen that some marginal improvement was achieved, mostly between $720\ Hz$ and $1120\ Hz$. For some frequencies, the PSD difference was up to $-5\ dB$, but for other frequencies, a rise of up to $2\ dB$ was produced. The right graph showed in Figure 14 shows the effect of plasma actuation on the pressure distribution affected by the vortices system. The peak of suction was slightly modified. At the region where the DBD-PAs were installed, the suction was augmented from x/c 0.4 to 0.7 at the suction side. The vortex was slightly intensified and shifted towards the leading edge.
In summary, the results obtained with the DBD-PAs installed at the flap rounded tip show that:

- DBD-PA applied to the rounded flap tip was more effective at lower Reynolds and Mach number, probably due to the small control authority of the DBD-PAs, as reported by other researchers

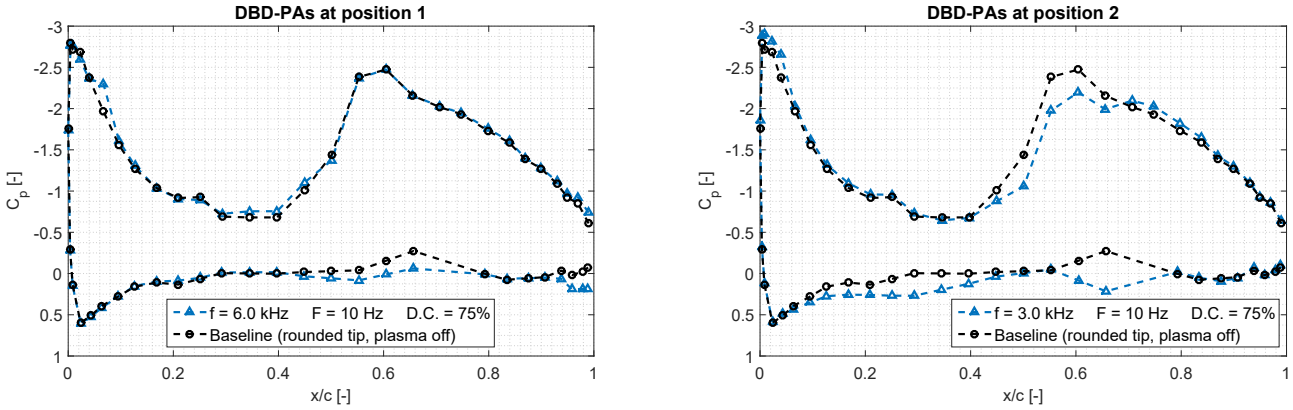

Figure 11 – Chordwise pressure distribution at the flap tip: DBD-PAs installed at position 1 (left) and 2 (right), $V_{in} = 30\ V$, $\alpha = 26°$, $Re = 1.12 \times 10^6$, $M = 0.08$.

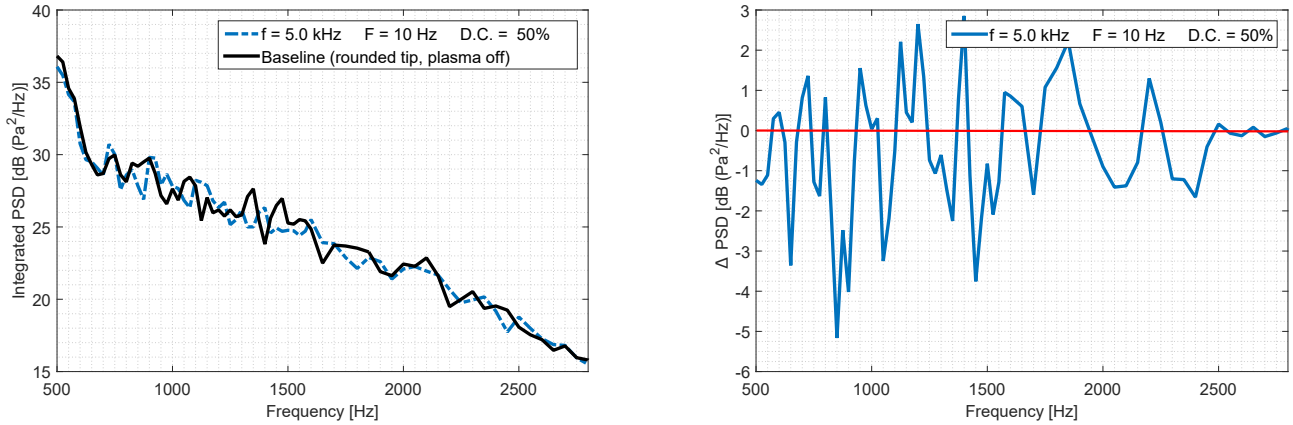

Figure 12 – Sound spectra: DBD-PAs installed at position 3, $V_{in} = 30\ V$ ($V_{pp} = 19.6\ kV$), $\alpha = 26°$, $Re = 5.76 \times 10^5$, $M = 0.04$.

(kinetic energy of the external flow is much greater than the kinetic energy introduced by the DBD-PA jet). This difference may also be related to a difference in the spanwise position of the DBD-PAs: in the most effective configurations, the DBD-PAs were installed in a position farther from the flap root.

- DBD-PA at the flap rounded tip has increased the OASPL for most configurations tested, but was able to marginally reduce the OASPL for some configurations, indicating its potential to affect the noise generation mechanism, since the pressure distribution over the flap tip was also affected by the DBD-PA activation (side-edge vortices were shifted). When compared to our tests of the use of DBD-PAs on the leading-edge slat [3], the use of DBD-PAs on the flap side-edge was less effective in reducing aerodynamic noise from high-lift devices.

4. Conclusions and suggestions for future works

The dielectric barrier discharge plasma actuators tested were able to marginally reduce the noise irradiated from the flap side-edge, showing its potential to directly interfere with the flap noise generation mechanisms. However, it was less effective in reducing aerodynamic noise than the application of DBD-PAs on the leading-edge slat. When applied to the flap side-edge together with a rounded tip, most of the configurations tested have increased the overall noise. However, when operated at 3.0 kHz and a duty cycle of 100%, it was able to reduce the overall sound pressure level in (0.75 $\pm$ 0.2) dB, by changing the vortices behavior. This performance could be increased by optimizing the DBD-PA electric circuit (impedance matching), materials, geometry, operational parameters, and manufacturing process. The authors believe, however, that in the current state of technology, the problems of plasma actuators do not outweigh the benefits and are far from being solved in order to

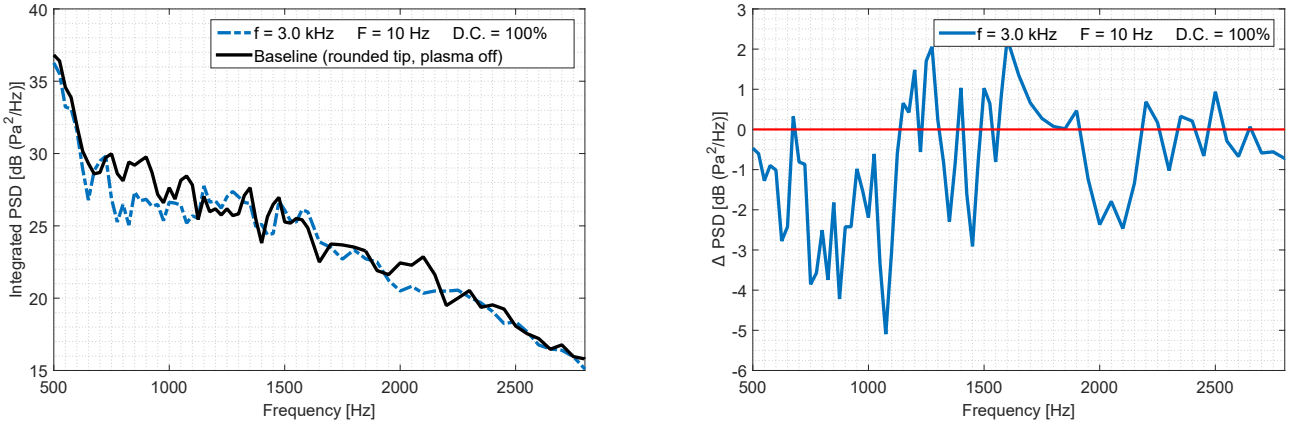

Figure 13 – Sound spectra: DBD-PAs installed at position 4, $V_{in} = 30\ V$ ($V_{pp} = 9.4\ kV$), $\alpha = 26°$, $Re = 5.76 \times 10^5$, $M = 0.04$.

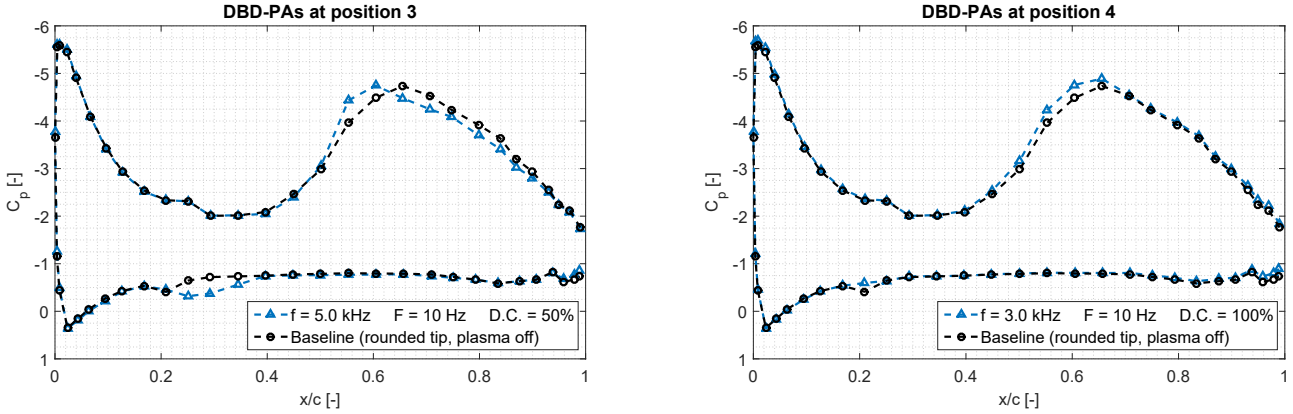

Figure 14 – Chordwise pressure distribution at the flap tip: DBD-PAs installed at position 3 (left) and 4 (right), $V_{in} = 30\ V$, $\alpha = 26°$, $Re = 5.76 \times 10^5$, $M = 0.04$.

transform the DBD-PAs into a feasible technical solution for applications in aviation. These problems are related mostly to the lack of robustness and of control authority of these devices at real scale flight conditions. The materials usually employed in the manufacture of DBD-PAs do not resist the exposure to plasma environments or to very high voltages without degrading, and DBD-PA performance is greatly affected by manufacturing defects. Besides, the presence of very high electric charges near fuel tanks creates a safety problem, mainly in case of rupture of the dielectric layer, when electric arcing is produced. Other problematic issues related to the DBD-PA applications are the generation of pollutant ozone and the emission of electromagnetic and acoustic actuation noises.

As suggestions for future works, further flow measurements should be carried out to enhance the understanding of the flow mechanisms responsible for the aeroacoustic phenomena presented in this paper. Electromagnetic noise and ozone produced by plasma actuators should also be measured to assess the negative side effects of operating these devices. The authors also advise that additional research on manufacturing methods and materials science should be performed to enable the production of more efficient plasma actuators.

5. Funding sources

This work was supported by the National Council for Scientific and Technological Development (CNPq) [grant number 148947/2017-4]; the Foundation for the Enhancement of Research and Industrial Improvement (FIPAI) [grant number FB-016/17]; the Funding Authority for Studies and Projects (FINEP); and Embraer.

6. Acknowledgments

The authors are grateful to the technicians José C. P. de Azevedo, Mário Sbampato and Osnan I. Faria, for their help in setting up and maintaining the experimental apparatus. The authors also acknowledge the engineers Daniel A. Giraldo, Laura B. Bolivar, and Lourenço T. L. Pereira, for their insights and their help in setting up and operating the experimental apparatus, and Dr. Carlos R. I. da Silva and Dr. Paulo C. Greco Júnior, for their contributions during the evaluation of the work presented hereby.

7. Contact Author Email Address

mailto: gabriel.gouveia.silva@alumni.usp.br

8. Copyright Statement

References

[1] Smith M J T. *Aircraft noise*. Cambridge University Press, 2009.

[2] Zaporozhets O, Attenborough K and Tokarev V. *Aircraft Noise*. CRC Press, 2011.

[3] Silva G P G, Eguea J P, Croce J A G and Catalano F M. Slat aerodynamic noise reduction using dielectric barrier discharge plasma actuators. *Aerospace Science and Technology*, Vol. 97, pp 105642, 2020.

[4] Turner T L, Kidd R T, Hartl D J and Scholten W D. Development of a SMA-based, slat-cove filler for reduction of aeroacoustic noise associated with transport-class aircraft wings. *ASME Conference on Smart Materials, Adaptative Structures and Intelligent Systems*, 2013.

[5] International Civil Aviation Organization. *Independent Expert Integrated Technology Goals Assessment and Review for Engines and Aircraft (Doc 10127)*. ICAO, 2019.

[6] Guo Y P and Joshi M C. Noise Characteristics of Aircraft High Lift Systems. *AIAA Journal*, Vol. 41, No.7, pp 1247-1256, 2003.

[7] Smith M and Chow S. Aerodynamic Noise Sources on Aircraft High Lift Slats and Flaps. *9th AIAA/CEAS Aeroacoustics Conference and Exhibit*, Reston, 2003.

[8] Kopiev V F, Zaytsev M Y, and Belyaev I V. Investigation of airframe noise for a large-scale wing model with high-lift devices. *Acoustical Physics*, Vol. 62, No. 1, pp 97-107, 2016.

[9] Khorrami M R. Understanding slat noise sources. *Computational Aeroacoustics: From Acoustic Sources Modeling to Far-Field Radiated Noise Prediction, EUROMECH Colloquium*, Vol. 449, pp 9-12, 2003.

[10] Chen P. *Identification and Attenuation of Slat Noise*. Doctoral thesis, University of Southampton, 2012.

[11] Dobrzynski W, Nagakura K, Gehlhar B, and Buschbaum A. Airframe noise studies on wings with deployed high-lift devices. *4th AIAA/CEAS Aeroacoustics Conference*, 1998.

[12] Imamura T, Ura H, Yokokawa Y, and Yamamoto K. A far-field noise and near-field unsteadiness of a simplified high-lift-configuration model (slat). *47th AIAA Aerospace Sciences Meeting Including the New Horizons Forum and Aerospace Exposition*, Reston, pp 1-15, 2009.

[13] Dobrzynski W. Almost 40 years of airframe noise research: What did we achieve? *Journal of Aircraft*, Vol. 47, No. 2, pp 353-367, 2010.

[14] Jenkins L, Khorrami M and Choudhari M. Characterization of unsteady flow structures near leading-edge slat: Part i: PIV measurements. *10th AIAA/CEAS Aeroacoustics Conference*, Reston, pp 1-15, 2004.

[15] Ma Z and Zhang X. Numerical investigation of broadband slat noise attenuation with acoustic liner treatment. *AIAA Journal*, Vol. 47, No. 12, pp 2812-2820, 2009.

[16] Choudhari M M and Khorrami M R. Slat cove unsteadiness: effect of 3d flow structures. *44th Aerospace Sciences Meeting and Exhibit*, Reston, pp 1-20, 2006.

[17] Khorrami M and Lockard D. Effects of geometric details on slat noise generation and propagation. *12th AIAA/CEAS Aeroacoustics Conference/27th AIAA Aeroacoustics Conference*, Reston, pp 1-28, Reston, 2006.

[18] Choudhari M M and Khorrami M R. Effect of three-dimensional shear-layer structures on slat cove unsteadiness. *AIAA Journal*, Vol. 45, No. 9, pp 2174-2186, 2007.

[19] Huang H, Li W P, and Wang F X. Slat noise suppression using upstream mass injection. *Journal of Shanghai Jiaotong University (Science)*, Vol. 18, No.5, pp 620-629, 2013.

[20] Dobrzynski W and Pott-Pollenske M. Slat noise source studies for farfield noise prediction. *7th AIAA/CEAS Aeroacoustics Conference and Exhibit*, 2001.

[21] Pereira L T L, Rego L F, Catalano F M, Reis D C, and Coelho E L C. Experimental slat noise assessment through phased array and hot-film anemometry measurements. *2018 AIAA Aerospace Sciences Meeting*, 2018.

[22] Lockard D and Choudhari M. Noise radiation from a leading-edge slat. *15th AIAA/CEAS Aeroacoustics Conference/30th AIAA Aeroacoustics Conference*, Reston, pp 1-16, 2009.

[23] Paschal K, Jenkins L, and Yao C. Unsteady slat wake characteristics of a 2-d high-lift configuration. *38th Aerospace Sciences and Meeting Exhibit*, Reston, Paper AIAA-2000-0139, 2000.

[24] Takeda K, Ashcroft G, Zhang X and Nelson P. Unsteady aerodynamics of slat cove flow in a high-lift device configuration. *39th Aerospace Sciences Meeting and Exhibit*, Reston, Paper AIAA-2001-0706, 2001.

[25] Huang X, Chan S, Zhang X, and Gabriel S. Variable structure model for flow-induced tonal noise control with plasma actuators. *AIAA Journal*, Vol. 46, No. 1, pp 241-250, 2008.

[26] Macaraeg M. Fundamental investigations of airframe noise. *4th AIAA/CEAS Aeroacoustics Conference/19th AIAA Aeroacoustics Conference*, Toulouse, pp 1-10, 1998.

[27] Drobietz R and Borchers I. Generic wind tunnel study on side edge noise. *12th AIAA/CEAS Aeroacoustics Conference*, Reston, 2006.

[28] Rossignol, K S S. Flow field measurements to characterize flap side-edge noise generation. *American Institute of Aeronautics and Astronautics Proceedings* , 2013.

[29] Hardin J C. Noise radiation from the side edges of flaps. *AIAA Journal*, Vol. 18, No. 5, pp 549-552, 1980.

[30] Acevedo D, Botero L, Lima Pereira L T, Catalano F, Reis D C and Coelho E L. Experimental aeroacoustic and aerodynamic analysis of a large-scale flap side-edge model. *2018 AIAA/CEAS Aeroacoustics Conference*, p. 3799, 2018.

[31] Imamura T, Ura H, Yokokawa Y, Enomoto S, Yamamoto K and Hirai T. Designing of slat cove filler as a noise reduction device for leading-edge slat. *13th AIAA/CEAS Aeroacoustics Conference*, Reston, 2007.

[32] Khorrami M R, Fares E, Duda B and Hazir A. Computational evaluation of airframe noise reduction concepts at full scale. *22th AIAA/CEAS Aeroacoustics Conference*, Red Hook, 2016.

[33] Giraldo D A. *Experimental Aeroacoustic and Aerodynamic Analysis of a Large-scale Flap Side-edge Model*. Master's thesis, University of São Paulo, 2019.

[34] Yong L, Xunnian W and Dejiu Z. Control strategies for aircraft airframe noise reduction. *Chinese Journal of Aeronautics*, Vol. 26, No. 2, pp 249-260, 2013.

[35] Moreau E. Airflow control by non-thermal plasma actuators. *Journal of Physics D: Applied Physics*, Vol. 40, No. 3, pp 605-636, 2007.

[36] Wang J J, Choi K S, Feng L H, Jukes T N and Whalley R D. Recent developments in DBD plasma flow control. *Progress in Aerospace Sciences*, Vol. 62, pp 52-78, 2013.

[37] Corke T C, Post M L and Orlov D M. SDBD plasma enhanced aerodynamics: concepts, optimization and applications. *Progress in Aerospace Sciences*, Vol. 43, No. 7-8, pp 193-217, 2007.

[38] Enloe C L, McLaughlin T, Font G I and Baughn J W. Parameterization of temporal structure in the single-dielectric-barrier aerodynamic plasma actuator. *AIAA Journal*, Vol. 44, No. 6, pp 1127-1136, 2006.

[39] Little J, Nishihara M, Adamovich I and Samimy M. High-lift airfoil trailing edge separation control using a single dielectric barrier discharge plasma actuator. *Experiments in Fluids*, Vol. 48, No. 3, pp 521-537, 2009.

[40] Zhang X, Li H X, Huang Y and Wang W B. Wing flow separation control using asymmetrical and symmetrical plasma actuator. *Journal of Aircraft*, Vol. 54 No. 1, pp 301-309, 2017.

[41] Enloe C L, McHarg M G and McLaughlin T E. Time-correlated force production measurements of the dielectric barrier discharge plasma aerodynamic actuator. *Journal of Applied Physics*, Vol. 103, No. 7, pp 073302, 2008.

[42] Roth J R, Sherman D M and Wilkinson S P. Boundary layer flow control with a one atmosphere uniform glow discharge surface plasma. *37th AIAA Aerospace Sciences Meeting and Exhibit*, Reston, 1998.

[43] Roth J R, Sherman D M, and Wilkinson S P. Electrohydrodynamic flow control with a glow-discharge surface plasma. *AIAA Journal*, Vol. 38, No. 7, pp 1166-1172, 2000.

[44] He C, Corke T C and Patel M P. Plasma flaps and slats: An application of weakly ionized plasma actuators. *Journal of Aircraft*, Vol. 46, No. 3, pp 864-873, 2009.

[45] Hasebe H, Naka Y and Fukagata K. An attempt for suppression of wing-tip vortex using plasma actuators. *Journal of Fluid Science and Technology*, Vol. 6, No. 6, pp 976-988, 2011.

[46] Silva G P G. *Dielectric barrier discharge plasma actuators applied to high-lift devices for aerodynamic noise reduction*. Master's thesis, Universidade de São Paulo, 2019.

[47] Catalano F M. The new closed circuit wind tunnel of the aircraft laboratory of university of São Paulo. *16th Brazilian Congress of Mechanical Engineering*, Vol. 6, pp 306-312, 2001.

[48] Catalano F M. The new closed circuit wind tunnel of the Aircraft Laboratory of University of Sao Paulo, Brazil. *24th International Congress of The Aeronautical Sciences*, Edinburgh, pp 1-8, 2004.

[49] Santana L D, Carmo M, Catalano F M and Medeiros M A F. The update of an aerodynamic wind-tunnel for aeroacoustics testing. *Journal of Aerospace Technology and Management*, Vol. 6, No. 2, pp 111-118, 2014.

[50] Fonseca W D, Ristow J P, Sanches D G and Gerges S N Y. A different approach to archimedean spiral equation in the development of a high frequency array. *SAE Technical Paper Series*, Paper 2010-36-0541, 2010.

[51] Pagani Júnior C C. *Aeroacoustic source mapping of a slat in a closed-section wind tunnel using beamforming with DAMAS deconvolution*. Doctoral thesis, University of São Paulo, 2014.

[52] Pereira L T. Experimental slat noise assessment by means of phased array and hot-film anemometry measurements. Master's thesis, University of São Paulo, São Carlos, 2018.